

18 U-SERIES ANALYSES OF BONES FROM MEGALOPOLIS BASIN SITES

Rainer Grün^{1,2,3}, Yuexing Feng², Jian-Xin Zhao², George E. Konidaris⁴, Athanassios Athanassiou⁵, Vangelis Tourloukis^{4,6}, Eleni Panagopoulou⁵, Panagiotis Karkanias⁷, Katerina Harvati^{3,4}

¹Research School of Earth Sciences, The Australian National University, Canberra, Australia

²School of Earth and Environmental Sciences, University of Queensland, Queensland, Australia

³DFG Centre for Advanced Studies 'Words, Bones, Genes, Tools', Eberhard Karls University of Tübingen, Tübingen, Germany

⁴Paleoanthropology, Institute for Archaeological Sciences and Senckenberg Centre for Human Evolution and Palaeoenvironment, Department of Geosciences, Eberhard Karls University of Tübingen, Tübingen, Germany

⁵Hellenic Ministry of Culture, Ephorate of Palaeoanthropology–Speleology, Athens, Greece

⁶Department of History and Archaeology, School of Philosophy, University of Ioannina, Ioannina, Greece

⁷M.H. Wiener Laboratory for Archaeological Science, American School of Classical Studies at Athens, Athens, Greece

*rwgruen@gmail.com

<http://dx.doi.org/10.15496/publikation-97644>

Keywords: U-series analysis; U-diffusion into bones; minimum age estimates

18.1 INTRODUCTION

The Megalopolis Basin (Peloponnese, Greece) hosted a large lake during the Pleistocene. Its sequence consists of fluviolacustrine deposits containing lignite seams. The paleolake sequence commences at ~900 ka and continued to ~150 ka, covering the late Early Pleistocene and the entire Middle Pleistocene (Tourloukis et al., 2018 and references therein). It offers the unique opportunity to investigate human activity in the basin and its environmental context through time, the goal of the MEGAPAL survey and CROSSROADS project (Harvati, this volume; Karkanias et al., this volume).

In order to shed light on the chronological framework of human activity and paleoenvironmental change in the Megalopolis Basin, we ap-

plied U-series analyses on bone samples from a series of archaeological and paleontological sites in the basin. Bone fragments of macro-mammals (37 specimens in total) were sampled from stratified contexts from four sites: Kyparissia-3 (8 specimens) and Kyparissia-4 (19 specimens) are located at the eastern part of the Kyparissia mine, and both yielded a rich vertebrate fauna (including mainly cervids, hippopotamuses and elephants), while Kyparissia-T (5 specimens), located in the southern part of the mine, represents mainly an accumulation of hippopotamus bones (Athanassiou et al., 2018). The previously known Kyparissia-4 paleontological locality was recently revisited by the CROSSROADS team, resulting not only in an expansion of its known faunal assemblage (Athanassiou, et al., this volume), but importantly in the identi-



<http://dx.doi.org/10.15496/publikation-97644>



R. Grün: <https://orcid.org/0000-0003-1366-3674>

J. Zhao: <https://orcid.org/0000-0002-2413-6178>

G. E. Konidaris: <https://orcid.org/0000-0002-7041-233X>

A. Athanassiou: <https://orcid.org/0000-0002-9140-7011>

V. Tourloukis: <https://orcid.org/0000-0002-9527-2708>

E. Panagopoulou: <https://orcid.org/0000-0002-4268-6157>

P. Karkanias: <https://orcid.org/0000-0002-7156-671X>

K. Harvati: <https://orcid.org/0000-0001-5998-4794>

fication of associated lithic artifacts (Karkanas et al., this volume). The fourth site, Tripotamos-4 (5 specimens), a newly discovered locality, is located at the southeastern corner of the Choremi mine and yielded a rich lithic assemblage together with some faunal remains, belonging mainly to cervids and bovids (Karkanas et al., this volume).

18.2 MATERIALS AND METHODS

18.2.1. U-SERIES DATING

The U-series results show a complex mixture of overprinting U-diffusion processes, which require a basic introduction to U-series analyses of bones. The bones of living organisms are virtually free of uranium, which helps to keep mutation rates down. Any uranium that is measured in fossil bones migrated into the bone after it was buried. If the U-uptake was a fast process, occurring shortly after burial, the calculated closed system U-series age is close to the burial age. However, if the diffusion process is ongoing or delayed, the calculated closed system U-series results underestimate the burial age by an unknown amount. Delayed strong U-uptake is often associated with hydrological changes, e.g., river incisions leading to an activation of the ground water circulation or changes in the precipitation regime. The calculated U-series results must therefore be regarded as minimum age estimates for the burial of the bone and actually indicate the timing of a U-uptake event. On top of this, U-leaching may occur, which complicates the interpretation of the results even further.

The basic principles of U-series measurements using laser ablation mass spectrometry and the interpretation of the results from bones were described by Grün et al. (2014). U-series dating is based on the fact that uranium (U^{6+}) is water soluble while thorium is not. Minerals precipitat-

ed from water contain U, but no Th. Within the ^{238}U decay chain, the activity ratio of ^{230}Th over ^{234}U is zero to start with. In addition, most waters contain an excess of ^{234}U over ^{238}U . With time the $^{230}Th/^{234}U$ activity ratio will increase until it reaches equilibrium ($^{230}Th/^{234}U=1$) after about 600 ka. Similarly, the $^{234}U/^{238}U$ ratio will decline until it reaches equilibrium ($^{234}U/^{238}U=1$). There is no straight algorithm for solving the age equation, this is done by iterations in a computer program. Graphically, it can be shown in an isotope evolution diagram (lower most panels of the Figures). The measured $^{230}Th/^{234}U$ and $^{234}U/^{238}U$ values are plotted into the diagram. The curved horizontal lines show the development of the $^{234}U/^{238}U$ ratio over time and the vertical lines give the age. Following the $^{234}U/^{238}U$ lines to the Y-axis yields the initial $^{234}U/^{238}U$ ratio ($^{234}U/^{238}U_0$) that was present in the U-source.

18.2.2. DIFFUSION ADSORPTION AND DIFFUSION ADSORPTION DECAY MODELS

Two models were developed for describing U-diffusion into bone: diffusion adsorption (DA; for details see Pike et al., 2002) and diffusion adsorption decay (DAD; Sambridge et al., 2012). Both treat bone as a homogeneous medium, thus are only applicable to dense bones. Looking at a cross section of a bone, the DA model predicts constant $^{234}U/^{238}U$ ratios and u-shaped U-concentration and age profiles. The model assumes that after an unspecified, but relatively short time after burial the system becomes closed (Pike, 2000). Thus, the afore-mentioned u-shaped age profiles will flatten out with time. If older samples are plotted in an isotope evolution diagram, they will form a cluster (see e.g., Fig. 2D). The DAD model assumes continuing U-diffusion. The U-concentration and age profiles are similar to those of the DA model, however, the $^{234}U/^{238}U$ ratios would also show a

u-shaped profile and the u-shaped age profiles are maintained over time, similar to Figs. 6F and G. In the isotope evolution diagram, the data would cross the $^{234}\text{U}/^{238}\text{U}$ evolution lines, as shown in Fig. 6H.

Leaching can be recognised by increasing ages towards the outside of the bone combined with decreasing U-concentrations. Data points that lie to the right of the $^{234}\text{U}/^{238}\text{U}$ lines in the isotope evolution diagram must have experienced U-leaching (e.g., Fig. 7D). Secondary overprints are characterised by lower ages at the outside (e.g., Fig. 2G). If the U-source of a secondary overprint has a different $^{234}\text{U}/^{238}\text{U}_0$ composition, these show up in the $^{234}\text{U}/^{238}\text{U}$ cross sections (e.g., Fig. 1B) and isotope evolution diagrams (e.g., Fig. 1D).

The samples were measured at the Radioisotope Laboratory at the School of Earth and Environmental Sciences, University of Queensland following the procedures described by Grün et al. (2014). All isotopes were measured simultaneously. The figures show examples of the various U-diffusion processes. All errors are $2\text{-}\sigma$. Averaged ages from a bone sequence were calculated from the integrated analytical results before converting them into a single age. No ^{232}Th corrections were carried out as all analyses had elemental U/Th ratios well in excess of 1000.

All samples from Kyparissia-T were from spongy bones and were not analyzed. The other three sites are discussed by their relative age according to their stratigraphical position (youngest to oldest).

18.3 RESULTS

18.3.1. TRIPOTAMOS-4

Figs. 1 and 2 show the results from four of the five bones from the site. TRP4-F29 (Figs. 1A to D) shows two distinct U-diffusion processes. To-

wards the outside, the $^{234}\text{U}/^{238}\text{U}$ ratios and U-concentrations increase while the $^{230}\text{Th}/^{234}\text{U}$ ratios and resulting ages decrease (Figs. 1B, C), indicating a secondary U-overprint. The process is clearly demonstrated in the isotope evolution diagram (Fig. 1D). The central data points cluster around 180 ka, but it cannot be ascertained whether these were also partly affected by the secondary overprint. Thus, it is not certain that this cluster presents the timing of an earlier distinct U-diffusion event. Note that the secondary overprint is very recent (Holocene). TRP4-F24 (Figs. 1E to H) shows an older section with higher $^{234}\text{U}/^{238}\text{U}$ ratios, lowering towards the outside (Figs. 1F). These regions are associated with increasing $^{230}\text{Th}/^{234}\text{U}$ ratios and decreasing U-concentrations (Figs. 1F, G), both signs of leaching. This is further demonstrated in the isotope evolution diagram with two data points in the leaching zone (Figs. 1H). The central data cluster has an average age of 206 ± 11 ka.

Samples TRP4-F20 and F31 (Fig. 2) behave significantly different to the previous two. TRP4-F20 (Fig. 2A to D) is the best-behaved sample of the whole data set. As there is no structure in the isotope ratio and age cross sections (Figs. 2B and C), continuous diffusion can be ruled out. The cluster in Fig. 2D represents a single diffusion event at 362 ± 43 ka. TRP4-F31 (Fig. 2E to H) shows a secondary overprint at the outside from a U-source with higher $^{234}\text{U}/^{238}\text{U}_0$ ratios. The rest of the data form a cluster at 466 ± 110 ka. A third sample (TRP4-F23), behaving similarly to F-31, contains a cluster at 368 ± 46 ka. The weighted mean of the three samples points to a U-mobilisation event at 365 ± 31 ka.

At Tripotamos-4 three distinct U-uptake events are recorded: the last during the Holocene (overprint in TRP4-F29), an earlier during MIS 7 (191 to 243 ka, MIS boundaries from Lisiecki and Raymo, 2005). The three older clusters may be the result of two uptake phases, one during MIS 9 (300 to 337 ka), the other during MIS 11 (374 to

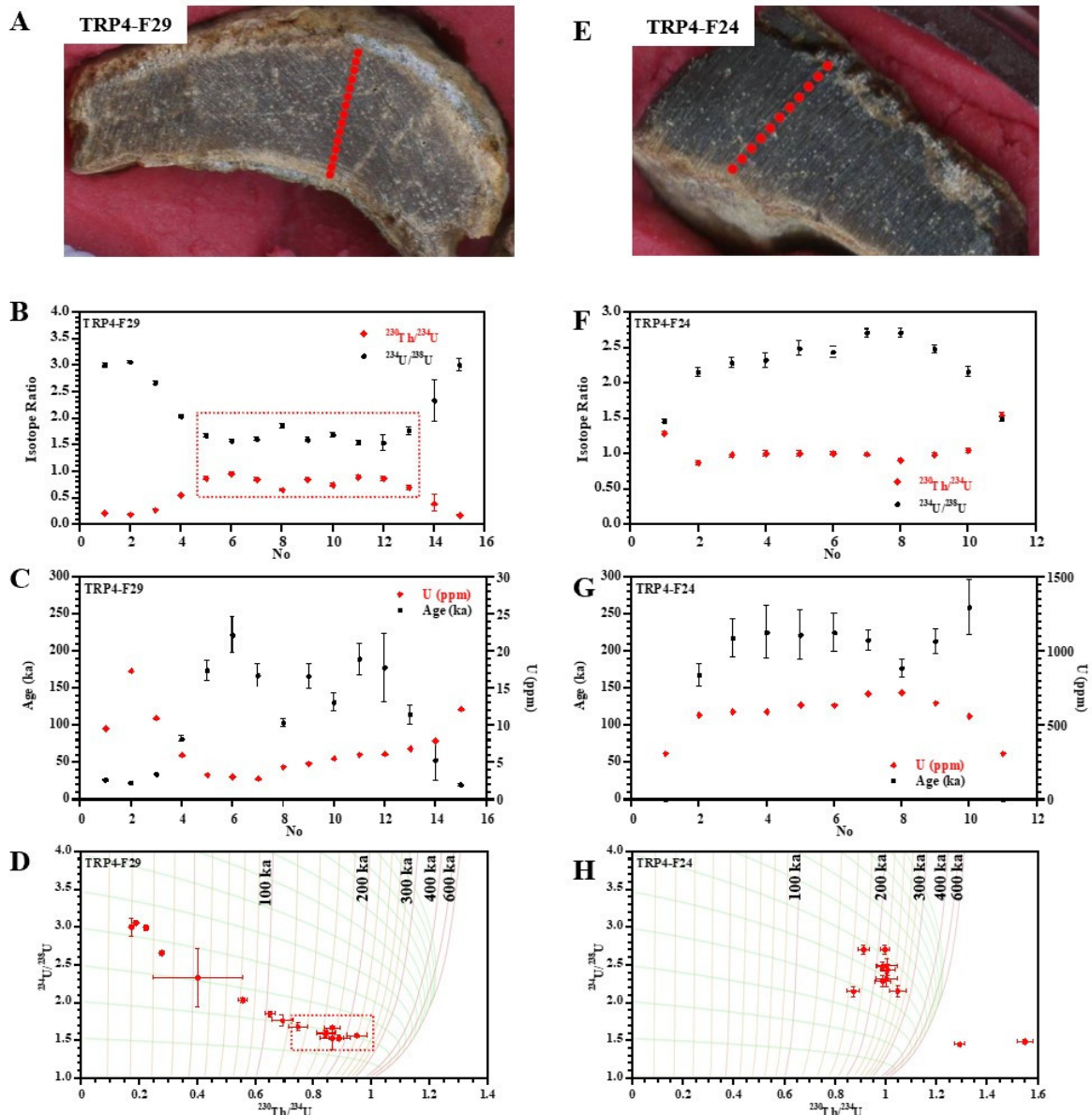


Figure 1: Results of TRP4-F29 and TRP4-F24 from Tripotamos-4. A, E: photos of the bone and location of the individual laser spot analyses; B, F: Plot of the measured $^{230}\text{Th}/^{234}\text{U}$ and $^{234}\text{U}/^{238}\text{U}$ ratios; C, G: calculated ages (left scale) and U-concentrations (right scale); D, H: isotope evolution diagrams.

424 ka), however, the data are not precise enough to make this distinction. The weighted mean is closer to MIS 11 but does not exclude MIS 9.

18.3.2. KYPARISSIA-3

Probably the most interesting sample from this site is KYP-901. It contains virtually no uranium: 0.25

ppm at the first data point and 0.09 ± 0.04 ppm for all others. This means that there are areas where no U-mobilisation took place for more than 400 ka. The presence of the lignite bands may be responsible for the complex U-history of the bones. The lignite redox reduces U^{6+} to U^{4+} , which is water insoluble. If waters run through a high redox area before reaching a bone, it may well be free of any uranium (as perhaps demonstrated by KYP-901).

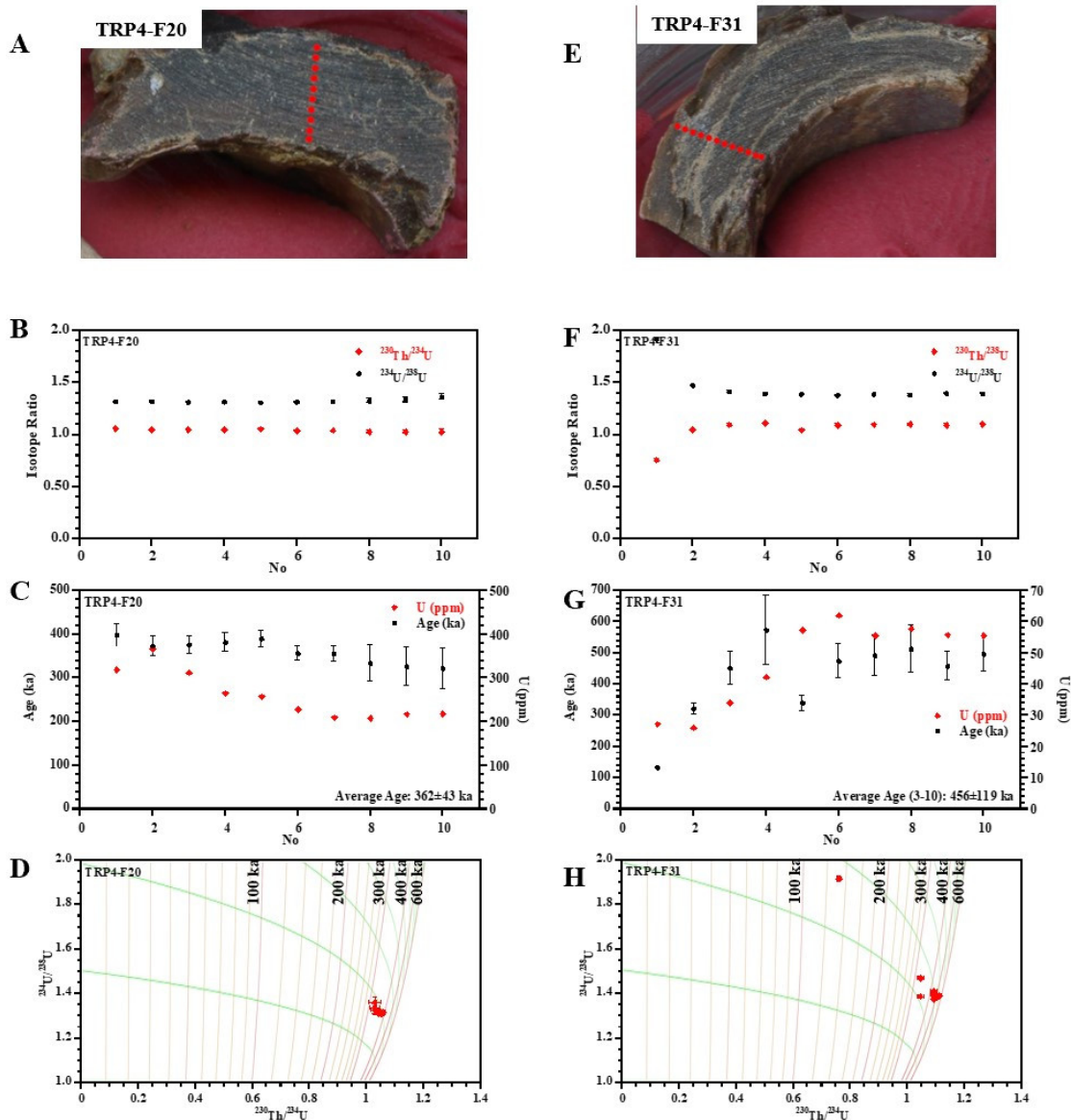


Figure 2: Results of TRP4-F20 and TRP4-F31 from Tripotamos-4. A, E: photos of the bone and location of the individual laser spot analyses; B, F: Plot of the measured $^{230}\text{Th}/^{234}\text{U}$ and $^{234}\text{U}/^{238}\text{U}$ ratios; C, G: calculated ages (left scale) and U-concentrations (right scale); D, H: isotope evolution diagrams.

KYP-131 (Figs. 3A to D) shows a secondary overprint at the outside. The rest clusters around 466 ± 121 ka, some of the scatter is probably due to uranium micro-migration within the bone (e.g., Duval et al., 2011). The data of KYP-18 (Figs. 3A to D) are in the same isotope range as KYP-131 but scatter more (compare Figs. 3D and H).

Sample KYP-94 (Fig. 4A to D) shows a secondary overprint at the outside with average age ages

of 204 ± 12 ka. The data further inside have large uncertainties because of the low U-concentrations, they average at 346 ± 89 ka. KYP-85 (Fig. 4E to H) shows the same overprint at the outside as KYP-94 at 205 ± 11 ka.

The remaining data have large uncertainties because of the low U-concentrations. The sample also shows a significant amount of leaching (Fig. 4H). Samples KYP-14A and B (Fig. 5) are from

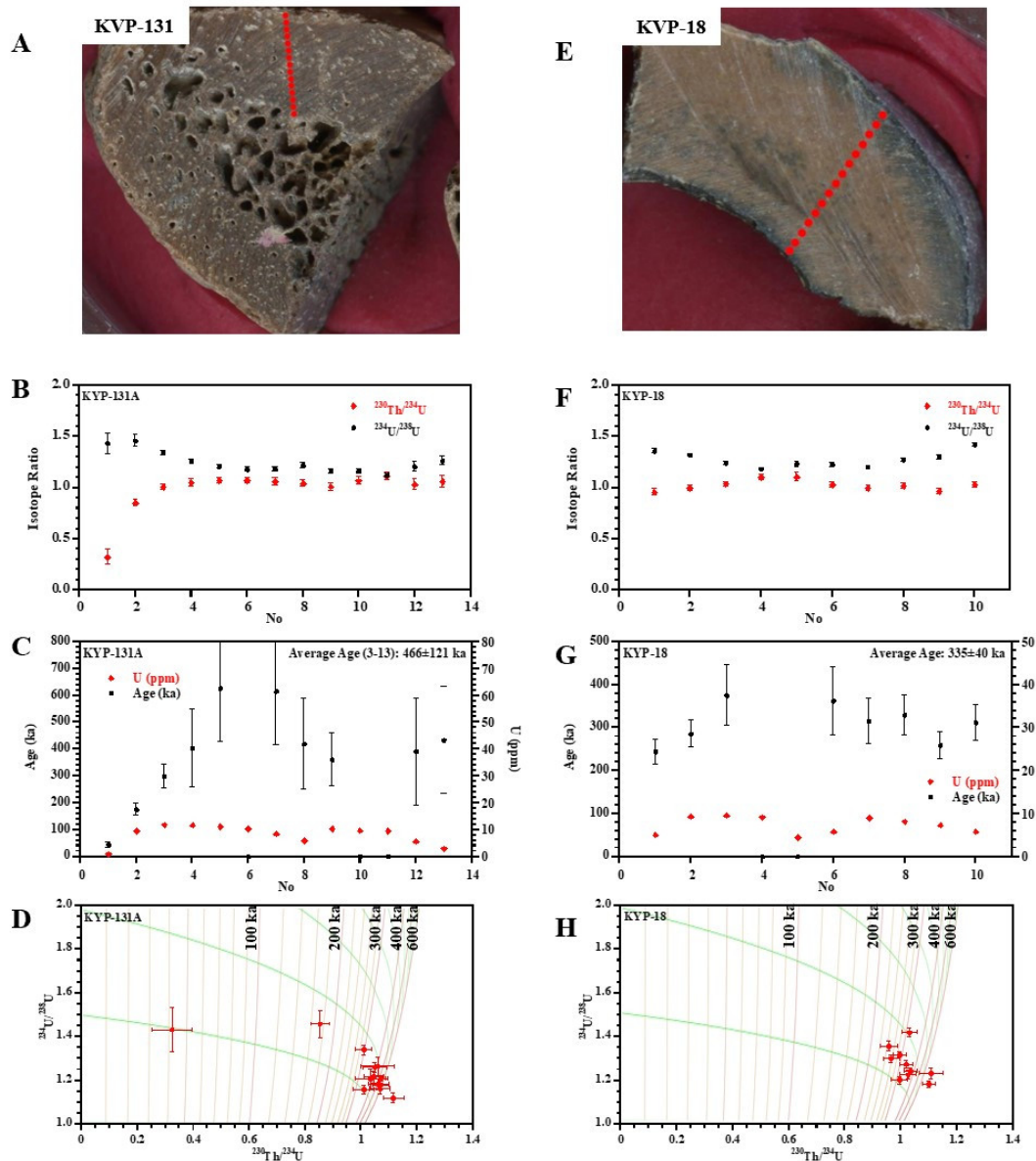


Figure 3: Results of KYP-131 and KYP-18 from Kyprisia-3. A, E: photos of the bone and location of the individual laser spot analyses; B, F: Plot of the measured $^{230}\text{Th}/^{234}\text{U}$ and $^{234}\text{U}/^{238}\text{U}$ ratios; C, G: calculated ages (left scale) and U-concentrations (right scale); D, H: isotope evolution diagrams.

the same bone. The data of KYP-14A (Fig. 5A to D) cluster tightly at 110 ± 4 ka with only the outer data point indicating a later overprint. The inner data points of sample KYP-14B (Fig. 5E to H) cluster around 114 ± 4 ka, relating to the same uptake event indicated in KYP-14A. The outer, older data points may relate to an earlier U-uptake event that diffused only into the outer section of the bone. This may be related to the 200 ka event

observed in KYP-85 and 94, but the apparent ages are somewhat younger because of mixing with the later U-diffusion.

The bones from Kyprisia-3 document three distinct U-uptake events at 110 ± 4 ka, 205 ± 8 ka and 347 ± 35 ka. The first two can be clearly associated with the interglacials of MIS 5 and MIS 7, while the one at 347 ± 35 ka may relate to MIS 9 (300 to 337 ka) or MIS 11 (374-424 ka).

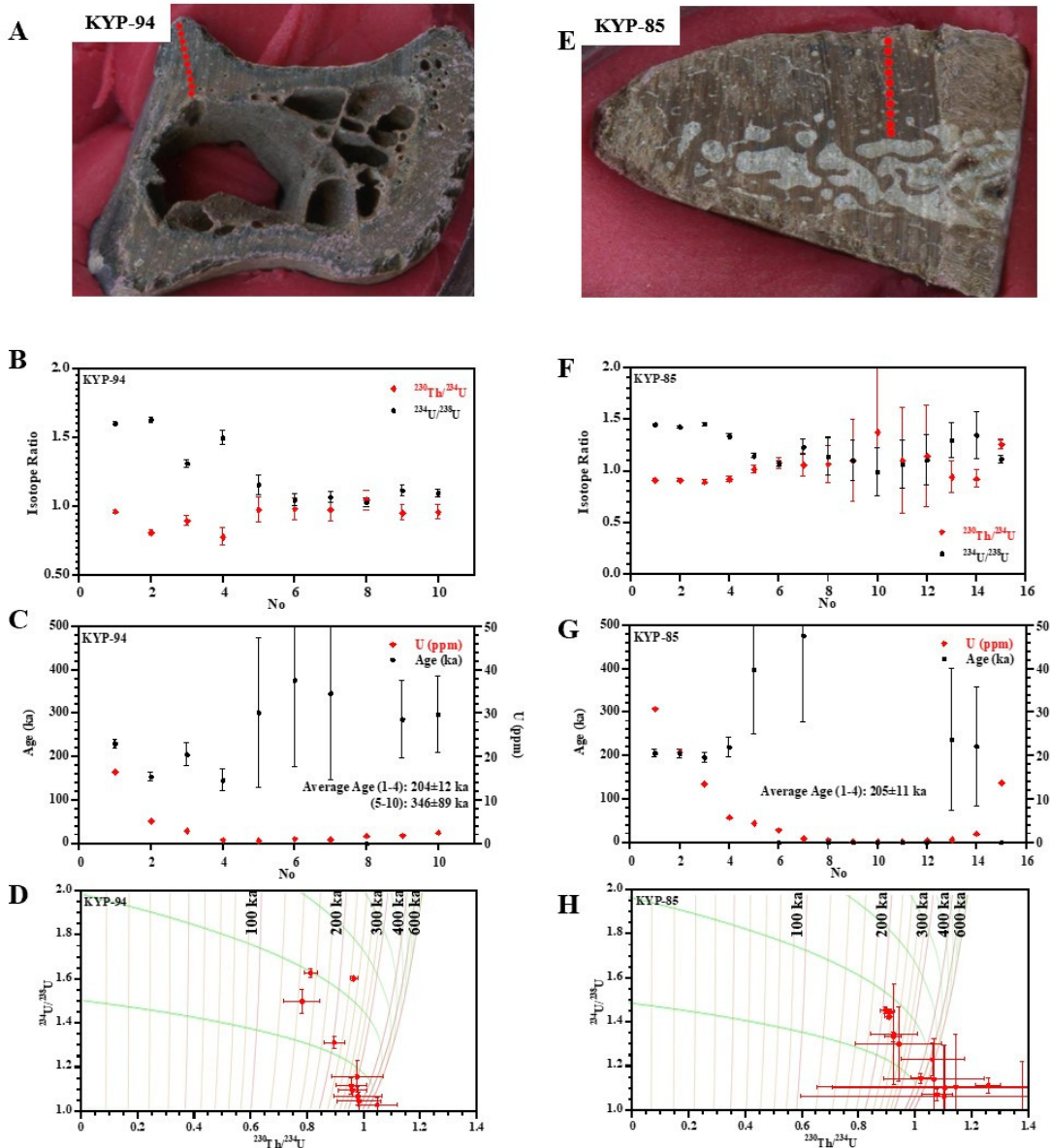


Figure 4: Results of KYP-94 and KYP-85 from Kyparissia-3. A, E: photos of the bone and location of the individual laser spot analyses; B, F: Plot of the measured $^{230}\text{Th}/^{234}\text{U}$ and $^{234}\text{U}/^{238}\text{U}$ ratios; C, G: calculated ages (left scale) and U-concentrations (right scale); D, H: isotope evolution diagrams.

18.3.3. KYPARISSIA-4

This is stratigraphically the oldest site. Virtually all samples show leaching. KYP4A-F125 (Fig. 6A to D) shows leaching at the inside surface, but also within the sample. The remaining data points cannot be explained by a simple diffusion process. It seems that two U-sources were operating with slightly different $^{234}\text{U}/^{238}\text{U}$ ratios, one slightly

above the $^{234}\text{U}/^{238}\text{U}_0$ evolution line and one slightly below (Fig. 6D). However, such sequences of data cannot be produced by diffusion in direction of the analysed transect (the data according to the DA model would cluster, according to the DAD model it would follow the direction of the blue data points in Fig. 6H). It could be explained by continuing diffusion into separate individual vol-

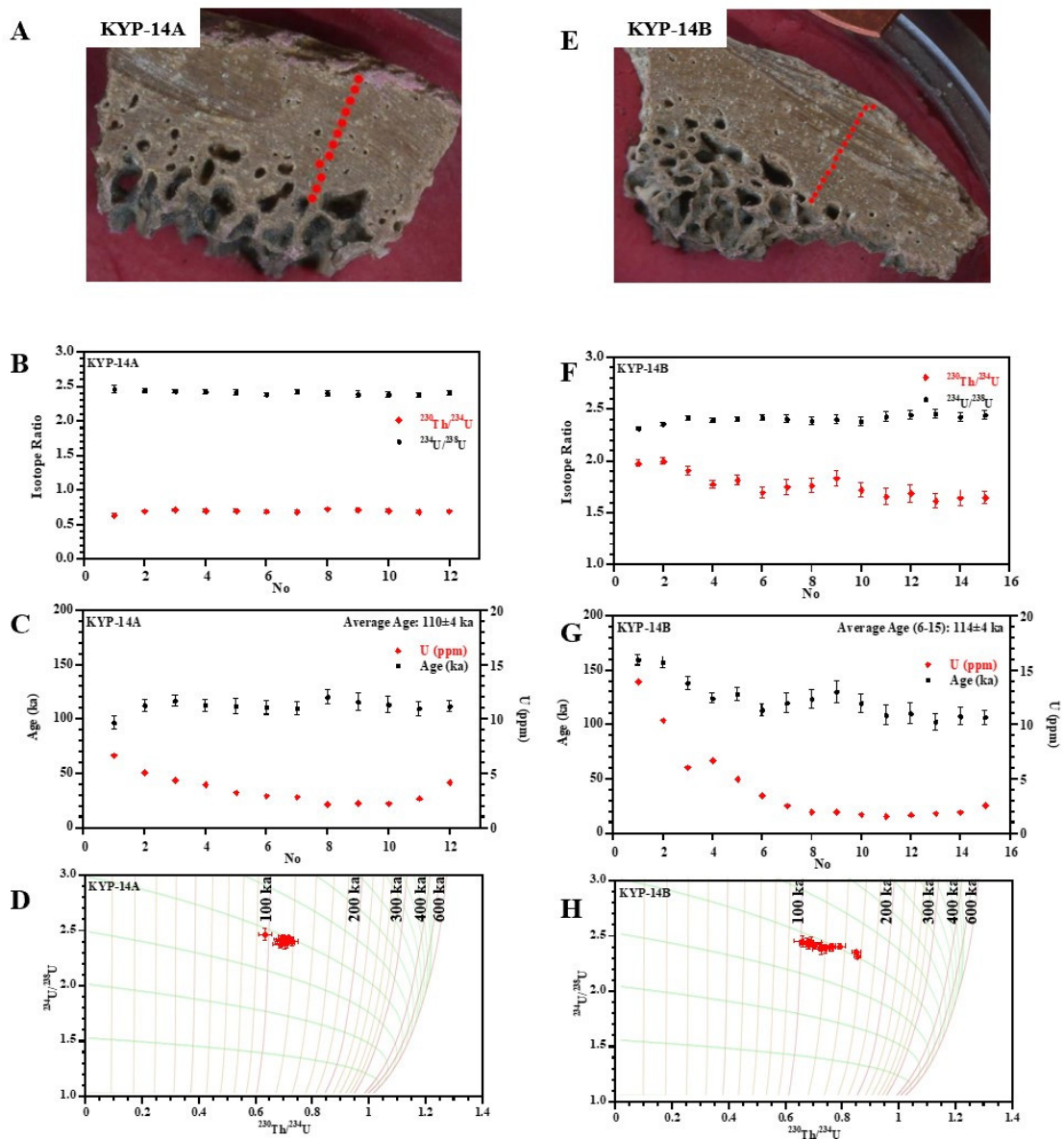


Figure 5: Results of KYP-14A and KYP-14B from Kyparissia-3. A, E: photos of the bone and location of the individual laser spot analyses; B, F: Plot of the measured $^{230}\text{Th}/^{234}\text{U}$ and $^{234}\text{U}/^{238}\text{U}$ ratios; C, G: calculated ages (left scale) and U-concentrations (right scale); D, H: isotope evolution diagrams.

umes, e.g., diffusion proceeding at a right angle to the transect. But this is speculative.

18.4 DISCUSSION

14 samples behaved similarly to KYP4A-F78 (Fig. 6E to H). At first glance, the samples show isotope distributions that are expected from the DAD

model: both the $^{234}\text{U}/^{238}\text{U}$ and $^{230}\text{Th}/^{234}\text{U}$ ratios show u-shaped profiles (Fig. 6F), the calculated ages and U-concentrations are also u-shaped. However, all samples have the highest U-concentrations at the outside and all samples show leaching (Fig. 6H). The relationship of increasing the $^{234}\text{U}/^{238}\text{U}$ ratios with increasing $^{230}\text{Th}/^{234}\text{U}$ ratios is the direct result of a continuing U-diffusion process (as postulated by the DAD model). The blue

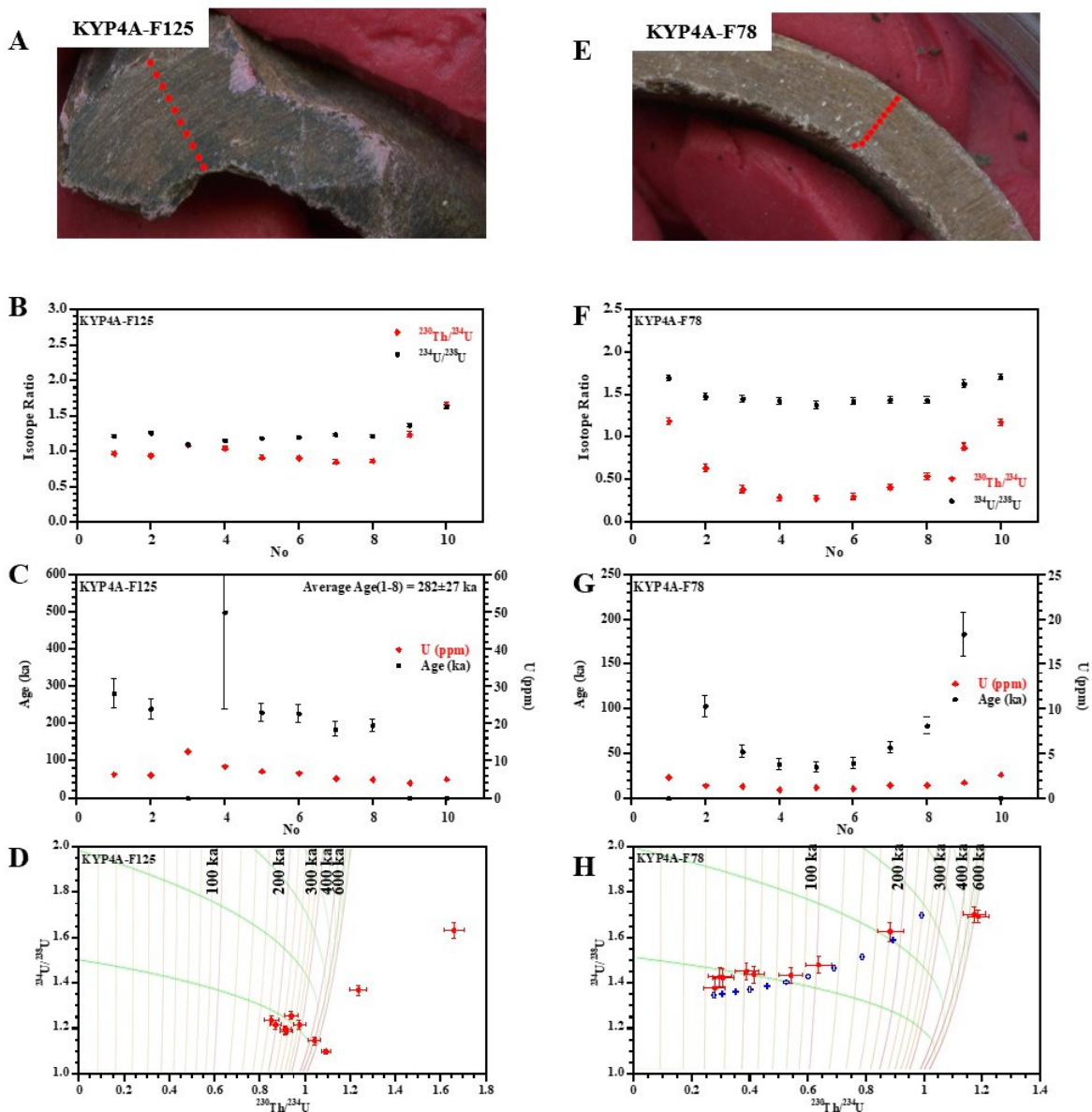


Figure 6: Results of KYP4A-F125 and KYP4A-F78 from Kyprisissia-4. A, E: photos of the bone and location of the individual laser spot analyses; B, F: Plot of the measured $^{230}\text{Th}/^{234}\text{U}$ and $^{234}\text{U}/^{238}\text{U}$ ratios; C, G: calculated ages (left scale) and U-concentrations (right scale); D, H: isotope evolution diagrams. The blue data points in Figure 6H are from a model calculation using the DAD diffusion model and data from Grün et al. (2014), their Figure 4.

data points in Fig. 6H result from a theoretical calculation of a 280 ka old sample using the data from Grün et al. (2014, their Fig. 4D). However, the analytical data of the bones from Kyprisissia-4 cannot be fitted by the DAD model as the extrapolation of the $^{234}\text{U}/^{238}\text{U}$ ratios towards the surfaces of the bone would require very large, unrealistic values. Fitting the central data points with the DAD model results in ages around 150 ka, with

very large uncertainties (the result for KYP4A-F78 was 154 ± 25 ka). It seems that the samples have undergone at least three U-diffusion stages: firstly, an uptake leaving u-shaped diffusion isotope and U-concentration profiles, then leaching, then a later overprint. The u-shaped isotope profiles may be the result of the mixing of the first uptake and a later overprint (this was also observed for an old sample from Melka Kunture, Grün et al. (2014),

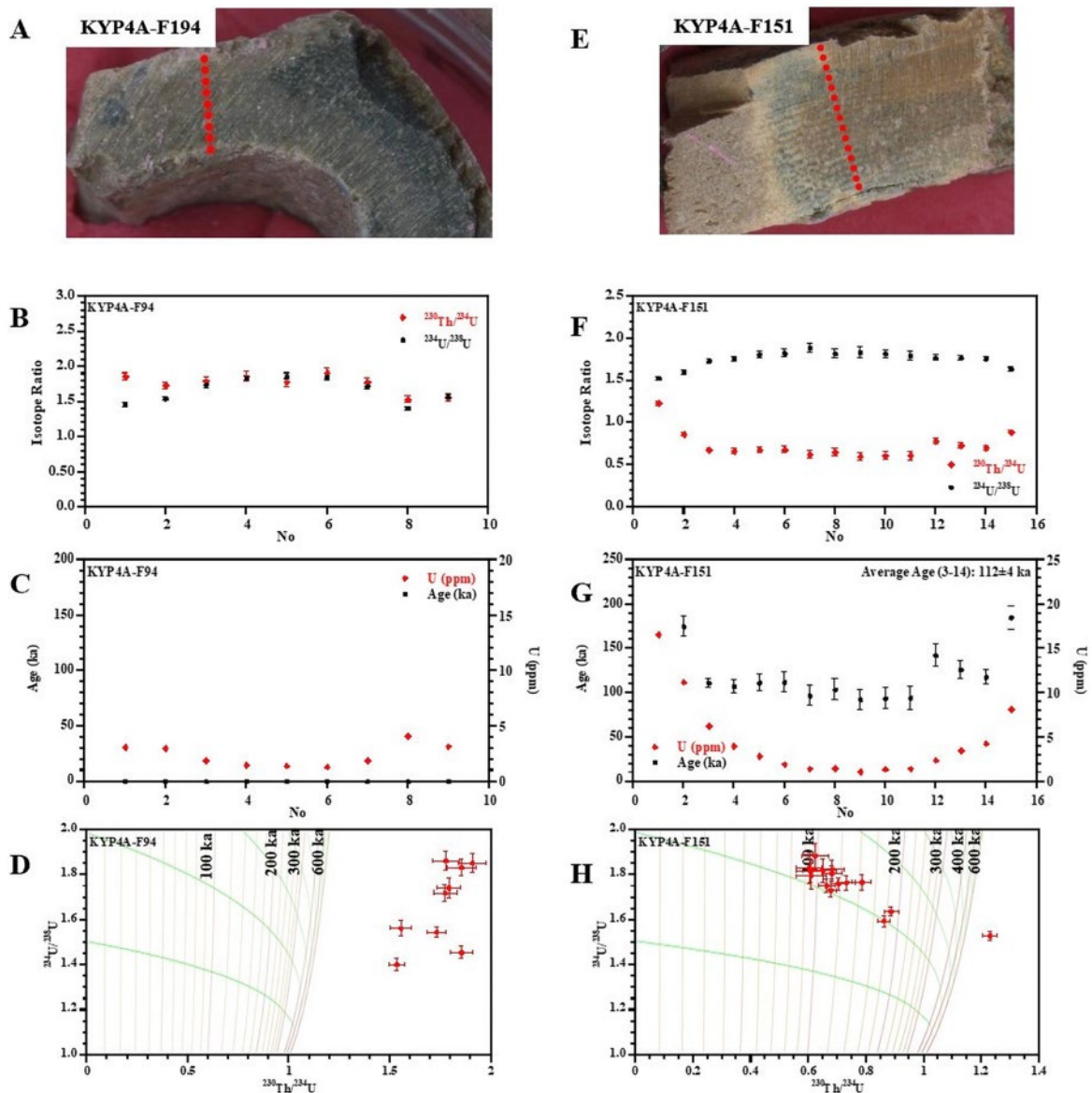


Figure 7: Results of KYP4A-F194 and KYP4A-F151 from Kyprisissia-4. A, E: photos of the bone and location of the individual laser spot analyses; B, F: Plot of the measured $^{230}\text{Th}/^{234}\text{U}$ and $^{234}\text{U}/^{238}\text{U}$ ratios; C, G: calculated ages (left scale) and U-concentrations (right scale); D, H: isotope evolution diagrams.

their Fig. 18). It is not possible to speculate when these processes took place.

Two samples showed massive leaching as shown by KYP4A-F194 (Fig. 7A to D). Note that the U-concentration profile is still u-shaped (Fig. 7C). Two other samples behaved like KYP4A-F151 (Fig. 7E to H) showing clusters around 100 ka and leaching towards the outside of the sample. The cluster of KYP4A-F151 has an average age of

112 ± 4 ka, that of the other sample (KYP4A-F106) was too scattered. The DA model predicts that the U-concentrations would decrease towards the outside as a result of leaching, but this is clearly not the case (Fig. 7G).

The bones from Kyprisissia-4 show a complex history of U-uptake and leaching processes. As frustrating as it is, only one sample allows the identification of a distinct uptake phase at 112 ± 4

ka. While it is clear that earlier continuing uptake processes took place, it is not possible to derive any age information from the data.

CONCLUSIONS

The U-series results on the bone samples from the Megalopolis Basin allow the identification of three distinct U-uptake phases corresponding to MIS 1, 5 and 7. Whether one or two distinct older uptake phases took place cannot be decided because of the large errors for the older data. The mean age of the older phases falls into the glacial of MIS 10 (337 to 374 ka). However, assuming that the U-diffusion events processes took place during an interglacial (as did the three later ones), the older U-accumulations took place either in MIS 9 or MIS 11, or both. The results give a minimum age of 365 ± 31 ka for Tripotamos-4 and 347 ± 35 ka for Kyparissia-3. The only tangible date of 112 ± 4 ka for Kyparissia-4 is not particularly helpful to tie down the age of this site. A combination of U-series and ESR dating on teeth could contribute to provide finite age estimates (Grün et al., 1988).

ACKNOWLEDGMENTS

This research was conducted under a permit granted to the Ephorate of Palaeoanthropology–Speleology, Hellenic Ministry of Culture, and the American School of Classical Studies at Athens. Fieldwork was supported by the ERC Consolidator Grant ERC-CoG-724703 (“CROSSROADS”) and the ERC Advanced Grant ERC-AdG-101019659 (“FIRSTSTEPS”), both awarded to K.H. We thank Q. Shao, College of Geography Science, Nanjing Normal University, for some IDAD calculations. We thank the anonymous reviewers for their constructive comments.

REFERENCES

- ATHANASSIOU, A., Michailidis, D., Vlachos, E., Turloukis, V., Thompson, N. and Harvati, K., 2018. Pleistocene vertebrates from the Kyparissia lignite mine, Megalopolis Basin, S. Greece: Testudines, Aves, Suiformes. *Quaternary International*, 497, pp. 178–197.
- ATHANASSIOU, A., Konidaris, G., Turloukis, V., Thompson, N., Giusti, D., Karkanias, P. and Harvati, K., this volume. The middle Pleistocene large mammal fauna from Kyparissia (Peloponnese, S. Greece): New collected material.
- DUVAL, M., Aubert, M., Hellstrom, J. and Grün, R., 2011. High resolution, LA-ICP-MS mapping of U and Th isotopes in an Early Pleistocene equid tooth from Fuente Nueva-3 (Orce, Andalusia, Spain). *Quaternary Geochronology*, 6, pp. 458–467.
- GRÜN, R., Schwarcz, H.P. and Chadam, J.M., 1988. ESR dating of tooth enamel: Coupled correction for U-uptake and U-series disequilibrium. *Nuclear Tracks and Radiation Measurements*, 14, pp. 237–241.
- GRÜN, R., Eggins, S., Kinsley, L., Mosely, H. and Sambridge, M., 2014. Laser ablation U-series analysis of fossil bones and teeth. *Palaeogeography, Palaeoclimatology, Palaeoecology*, 416, pp. 150–167.
- HARVATI, K., this volume. Introduction to the volume.
- KARKANAS, P., Turloukis, V., Thompson, N., Giusti, D., Tsartsidou, G., Athanassiou, A., Konidaris, G., Roditi, E., Panagopoulou, E. and Harvati, K., this volume. The Megalopolis Paleoenvironmental Project (MegaPal).
- LISIECKI, L.E., Raymo, M.E., 2005. A Pliocene – Pleistocene stack of 57 globally distributed benthic $\delta^{18}\text{O}$ records. *Paleoceanography*, 20(1).
- PIKE, A.W.G., 2000. Uranium series dating of archaeological bone by thermal ionization mass

- spectrometry. Doctoral dissertation, University of Oxford, UK.
- PIKE, A.W.G., Hedges, R.E.M. and Van Calsteren, P., 2002.** U-series dating of bone using the diffusion-adsorption model. *Geochimica et Cosmochimica Acta*, 66, pp. 4273–4286.
- SAMBRIDGE, M., Grün, R. and Eggins, S., 2012.** U-series dating of bone in an open system: The diffusion-adsorption decay model. *Quaternary Geochronology*, 9, pp. 42–53.
- TOURLOUKIS, V., Muttoni, G., Karkanas, P., Monesi, E., Scardia, G., Panagopoulou, E. and Harvati, K., 2018.** Magnetostratigraphic and chronostratigraphic constraints on the Marathousa 1 Lower Palaeolithic site and the Middle Pleistocene deposits of the Megalopolis Basin, Greece. *Quaternary International*, 497, pp. 154–169.